# Investigation of the near-infrared spectral character of putative Martian chloride deposits

Heidi B. Jensen[1] and Timothy D. Glotch[1]

Received 13 June 2011; revised 12 September 2011; accepted 4 October 2011; published 20 December 2011.

[1] Putative chloride salt deposits observed throughout the southern highlands of Mars by the Compact Reconnaissance Imaging Spectrometer for Mars (CRISM) display featureless red slopes in near-infrared ratio spectra. It is hypothesized that the admixture of anhydrous chlorides or unoxidized sulfides with silicate rocks or minerals could imitate this spectral behavior. Three different sets of spectra were collected: (1) simple mixtures of halite with labradorite and flood basalt at multiple concentrations, (2) halite crusts formed on both labradorite and flood basalt, and (3) simple mixtures of 25 and 50 wt % acid-washed pyrite with labradorite and flood basalt. In all three instances, multiple grain sizes were used to evaluate the effect of particle size on spectral results. Spectra of the mixtures and crusts were divided by pure labradorite and flood basalt spectra of the same grain size to produce ratio spectra comparable to the CRISM ratio spectra. Our study rules out pyrite as a possible component of these deposits, whereas flood basalt mixtures with halite reproduced the observed red slope under some conditions. This allows us to place some broad constraints on halite proportions and the effective grain sizes of these deposits.

**Citation:** Jensen, H. B., and T. D. Glotch (2011), Investigation of the near-infrared spectral character of putative Martian chloride deposits, *J. Geophys. Res.*, *116*, E00J03, doi:10.1029/2011JE003887.

## 1. Introduction

[2] The presence of putative chloride salt-rich deposits in the southern highlands of Mars was originally observed in Mars Odyssey Thermal Emission Imaging System (THEMIS) daytime midinfrared images. These features display a blue slope in the 7.93–12.57 $\mu$m region compared to the surrounding terrain. The deposits can be easily identified by their distinctive aqua color in THEMIS band 9, 6, 4 (12.57, 10.21, and 8.56 $\mu$m, respectively) decorrelation stretched (DCS) images [*Gillespie et al.*, 1986; *Osterloo et al.*, 2008, 2010; *Glotch et al.*, 2010]. Data covering these deposits from the Compact Reconnaissance Imaging Spectrometer for Mars (CRISM) instrument on board the Mars Reconnaissance Orbiter (MRO) also display a unique spectral character in the near-infrared (NIR) spectral range in overlapping full resolution targeted (FRT) and half resolution long (HRL) targeted images [*Murchie et al.*, 2009; *Wray et al.*, 2009; *Glotch et al.*, 2010]. These putative chloride-rich units exhibit featureless spectra in CRISM L spectrometer NIR data, with a red slope in the 1.1–2.6 $\mu$m range and an inverted hydration feature in the 3 $\mu$m region when ratioed to a spectrally neutral region within the CRISM image. Throughout the southern highlands of Mars, many occurrences of smectite clays are found adjacent to these units of interest, suggesting that these sites were in contact with liquid water over long time periods [*Murchie et al.*, 2009; *Wray et al.*, 2009]. In Terra Sirenum, where the largest co-occurrence of phyllosilicates and putative chlorides are observed on Mars, CRISM data also reveal the presence of vermiculite and/or a smectite/chlorite interlayer clay in close association with the putative chloride-rich material, suggesting that diagenesis occurred after initial phyllosilicate deposition [*Milliken and Bish*, 2010; *Glotch et al.*, 2010]. The occurrence of these mineral assemblages suggests a diverse aqueous history in which parts of the ancient Noachian crust were altered by liquid water [e.g., *Wray et al.*, 2009].

[3] Some unoxidized sulfides and anhydrous chlorides exhibit featureless spectra throughout the spectral range of both THEMIS and CRISM [*Hunt et al.*, 1971; *Hunt et al.*, 1972]. Whereas unaltered sulfides are unlikely to exist in close proximity to phyllosilicate deposits, they have yet to be ruled out spectrally. Sulfide minerals would most likely be oxidized and converted to sulfates upon persistent exposure to aqueous weathering processes at the surface of Mars [*Burns and Fisher*, 1993; *Zolotov and Shock*, 2005]. Both unoxidized sulfides and anhydrous chloride salts lack red slopes in the 1.1–2.6 $\mu$m region in laboratory spectra (Figure 1), suggesting that this characteristic in CRISM ratio spectra could be the result of an admixture of anhydrous chloride salts or unoxidized sulfides with the surrounding materials (see R. N. Clark et al., USGS digital spectral library splib06a, U.S. Geological Survey, Digital Data Series 231, http://speclab.cr.usgs.gov/spectral.lib06/). In this work, we acquired NIR (1.1–2.5 $\mu$m) spectra of mixtures of halite and pyrite with labradorite and flood basalt standards. The

[1]Department of Geological Sciences, State University of New York at Stony Brook, Stony Brook, New York, USA.


0148-0227/11/2011JE003887

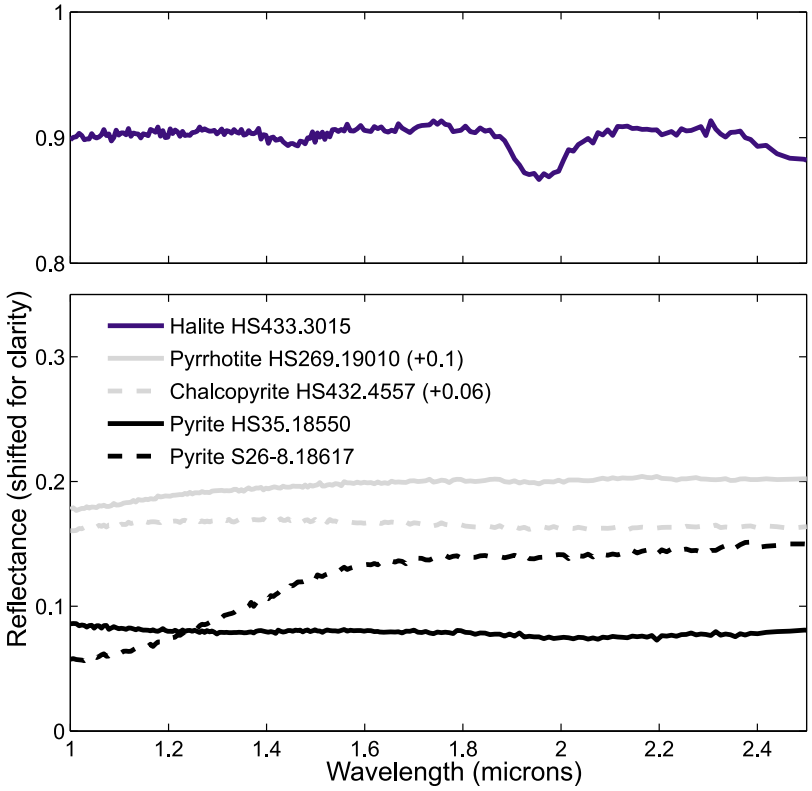


**Figure 1.** NIR reflectance spectra of halite, pyrrhotite, chalcopyrite, and two pyrites from the U.S. Geological Survey (USGS) spectral library (available at http://speclab.cr.usgs.gov/spectral.lib06/). Absorptions in the halite spectrum centered at 1.4 and 1.9 $\mu$m are hydration features.

goals of this study are to determine if chloride salts or sulfides mixed with these silicate phases can reproduce the featureless, red-sloped spectra observed in CRISM data.

## 2. Background

### 2.1. Halite

#### 2.1.1. Halite on Earth

[4] Terrestrial chloride deposits form by (1) precipitation from an evaporating or freezing surface composed of surface water, groundwater, or hydrothermal brines; (2) crystallization directly onto sediment grains (efflorescence); or (3) condensation of volcanic gases [*Bernard and Le Guern*, 1986; *Symonds et al.*, 1987; *Goodall et al.*, 2000]. Playas are a well-studied and common terrestrial environment in which massive evaporitic deposits, including chloride salts, can be observed due to alternating wet and dry periods, high evaporation rates and their hydrologic isolation in closed basins [*Hardie et al.*, 1978]. The brine compositions of terrestrial saline lakes (CaMgNa(K)Cl, Na(Ca)$SO_4$Cl, MgNa(Ca)$SO_4$Cl, $NaCO_3$Cl, and $NaCO_3SO_4$Cl) and subsequent precipitates are dependent on the chemical weathering reactions produced by the inflowing waters. The ubiquitous presence of sodium in these brines results from the weathering of feldspars, the dissolution of halite and some atmospheric sources [*Hem*, 1992; *Eugster and Hardie*, 1978]. The first minerals to precipitate from an evaporating brine are generally carbonate and gypsum followed only much later in brine evolution by halite and other chlorides due to their extremely high solubilities [*Eugster and Hardie*, 1978]. These evaporitic environments can result in spatially extensive, thick chloride deposits such as those found in Death Valley, California.

[5] Whereas terrestrial saline lakes are a large source, volcanic sublimates from fumaroles are also a source of chloride salt deposition. In condensation studies conducted using fumarole gases of Mount St. Helens in Washington state and the Merapi Volcano in Indonesia, gases emitted were condensed in silica tubes resulting in the deposition of both halite and sylvite in the range of 550–450°C [*Bernard and Le Guern*, 1986; *Symonds et al.*, 1987]. At higher temperatures, magnetite, cristobalite, molybdenite, and ferberite crystalized and at lower temperatures sulfides, including greenockite (CdS) and galena (PbS) condensed out of the gaseous phase [*Bernard and Le Guern*, 1986]. Whereas fumaroles result in the deposition of chloride minerals, deposits from these sources are not laterally or vertically extensive.

#### 2.1.2. Halite in Shergottite, Nakhlite, and Chassignite Meteorites

[6] Only two of the 99 approved SNC (shergottite, nakhlite, and chassignite) meteorites, Nakhla and Shergotty, possess secondary mineralogy that includes the presence of halite based on petrographic observations [*Gooding et al.*, 1990, 1991; *Bridges et al.*, 2001]. In Nakhla, halite is present as (1) an interstitial component with segregated clusters of one or more crystals of up to 400 $\mu$m in size, (2) a coating with anhydrite covering plagioclase and silica grains, and (3) the filling of veins in association with siderite and anhydrite adjacent to interstitial areas [*Bridges and Grady*, 1999; *Bridges et al.*, 2001]. *Bridges and Grady* [2000] suggested a progressive evaporation model in which the

secondary mineralogy corresponds with the extent of evaporation where Lafayette, Governador Valadares and Nakhla have >20%, 15–20%, and <10% water remaining. All three nakhlites contain goethite and apatite, with Lafayette representing the initial precipitates from the brine with Ca-rich siderite and smectite/illite followed by Governador Valadares which has siderite, smectite/illite, gypsum, and anhydrite followed by the final stage of precipitation in Nakhla with Mg, Mn-rich siderite, smectite/illite, halite, and $MgSO_4$. In Shergotty, minor isolated occurrences of Mg-chloride are present with halite as the dominant chloride occurring as vein filling material, a covering of silicate surfaces in rounded patches, and variably weathered individual or clumped halite grains [*Wentworth et al.*, 2000]. *Bridges et al.* [2001] suggested that the source of this secondary mineralogy in both Nakhla and Shergotty is the evaporation of low-temperature (25–150°C) brines. Their study also suggests that the presence of high sulfur and chloride concentrations in Martian soils may have resulted from the redistribution of these deposits by aeolian processes.

#### 2.1.3. In Situ Observation of Halogens on Mars

[7] Through data collected by the X-ray fluorescence spectrometers (XRF) aboard the two Viking landers, the alpha proton X-ray spectrometer (APXS) aboard Pathfinder's Sojourner and the alpha particle X-ray spectrometers (APXS) aboard the Mars Exploration Rovers (MER), we have been able to collect geochemical data, including Cl and Br concentrations, at the Martian surface. From the 17 samples analyzed with high precision from Chryse Planitia (Viking Lander 1) and Utopia Planitia (Viking Lander 2), Viking XRF data suggest that Martian fines have higher concentrations of Cl than terrestrial soils, with a range of 0.3–0.9 wt % [*Clark et al.*, 1982]. Data collected from the soils and rocks of Ares Vallis by the APXS instrument on the Sojourner rover revealed a mean value of 0.55 wt % Cl in Pathfinder soils and a calculated value of 0.32 wt % chloride for soil-free rocks [*Brückner et al.*, 2003]. In the first 1368 sols of the Spirit rover's journey, the APXS instrument observed 0.1–1.9 wt % Cl in the soils and rocks of the Gusev plains and Columbia Hills [*Gellert et al.*, 2006; *Ming et al.*, 2008]. In the first 90 sols of the Opportunity rover's travels, its APXS revealed Cl concentrations in the rocks ranging 0.06–0.44 wt % on surfaces on which the rock abrasion tool (RAT) was used and 0.54–0.68 wt % on unabraded surfaces. Opportunity's APXS also revealed Cl concentrations in the Meridiani Planum soils ranged from 0.33 to 0.54 wt % [*Rieder et al.*, 2004].

[8] Aqueous chemical analyses of the northern plains of Vastitas Borealis by the Wet Chemistry Laboratory (WCL) on the Phoenix Mars Lander indicate that Cl is present in perchlorate minerals in this region of Mars [*Hecht et al.*, 2009]. This detection of perchlorate in the soils at the Phoenix lander site brings to question the source of elemental Cl detections by the other rover missions. Whereas the Viking, Sojourner, MER Opportunity and Spirit rovers all detected Cl in the soils and rocks that they analyzed, some proportion of that Cl could be held in perchlorates and not chloride minerals.

### 2.2. Sulfides

#### 2.2.1. Sulfides on Earth

[9] On Earth, sulfides are present as components of hydrothermal veins (e.g., black smokers), pegmatites, contact metamorphic deposits, and stratiform sedimentary environments [*Deer et al.*, 1992]. Sulfide mineral deposits in the form of stratabound lenses or sheets with thicknesses of up to a few meters can be found at the base of magnesian ultramafic lava flows (komatiites) and have been proposed to be present on Mars as well [*Guilbert and Park*, 1986; *Burns and Fisher*, 1990]. Upon exposure of sulfide minerals to the surface by mining practices or uplift, interaction with surficial oxygenated water results in oxidation to form a large array of sulfate minerals and oxyhydroxides as well as acidification of surface waters [*Jambor et al.*, 2000]. Gossans, which are capping units composed mainly of iron oxides and quartz, are formed when ore deposits containing sulfide minerals interact with cyclic surface water, leaching sulfides and primary ore materials, resulting in supergene enrichment at depth [*Guilbert and Park*, 1986].

#### 2.2.2. Sulfides in SNCs

[10] Sulfides are present in SNC meteorites as minor components. An array of Fe-sulfides have been observed, including pyrrhotite ($Fe_{(1-x)}S$ (x = 0 to 0.2)), troilite ($Fe_7S_8$, also given as $Fe_{(1-x)}S$), pyrite ($FeS_2$), chalcopyrite ($CuFeS_2$), pentlandite ($(Fe,Ni)_9S_8$, and marcasite ($FeS_2$) as minor accessory phases in SNC meteorites in petrographic studies [*McSween*, 1985]. A stepped combustion experiment performed on Shergotty, ALHA 77005, Chassigny, and Nakhla produced concentrations of sulfur as sulfide ranging from 75 ppm in Nakhla to 1665 ppm in Shergotty with bulk sulfur ranging from 220 to 1930 ppm [*Burgess et al.*, 1989]. A study of 6 shergottites, including 2 olivine-phyric and 4 basaltic shergottites, via electron microprobe revealed ranges of sulfide from 0.16 to 0.53 area % [*Lorand et al.*, 2005].

#### 2.2.3. In Situ Observations of Sulfur on Mars

[11] X-ray spectrometer data from NASA's landers and rovers on the Martian surface have provided information about the overall sulfur concentration of soils and rocks. The 17 samples with high-precision analysis collected from both Viking lander sites revealed that (1) Martian fines have higher concentrations of sulfur than soils on Earth, (2) sulfur is positively correlated with chlorine, and (3) sulfur accounts for 5.9–9.5% of the elemental composition of the fines as $SO_3$ [*Clark et al.*, 1982]. The Mars Pathfinder Sojourner rover APXS revealed the mean S content of soils at 2.7 wt %, cemented soil at 2.5 wt % and the calculated soil-free rock at 0.3 wt % [*Brückner et al.*, 2003]. The Spirit rover revealed S concentrations ranging from 1.09 to 35.1 wt % sulfur as $SO_3$ from the beginning of its mission to sol 1368 [*Gellert et al.*, 2006; *Ming et al.*, 2008]. In comparison, data from the first 90 sols of the Opportunity rover data collection revealed 4.52–7.29 wt % sulfur as $SO_3$ [*Rieder et al.*, 2004]. It should be noted that all elemental values of sulfur on the surface collected by rover instruments have been reported as $SO_3$.

[12] A few in situ observations of unoxidized sulfide were observed by the Mössbauer instruments aboard the Opportunity and Spirit rovers. Based on Mössbauer data collected by the Opportunity rover, the stony-iron meteorites Barberton, Santa Catarina, Santorini and Kasos are inferred to contain troilite [*Schröder et al.*, 2008, 2010; *Fleischer et al.*, 2010]. These four stony-iron meteorites have been paired based on their chemical and mineralogical similarities, despite being observed over a distance of ~10 km in Opportunity's roving path [*Schröder et al.*, 2008, 2010;

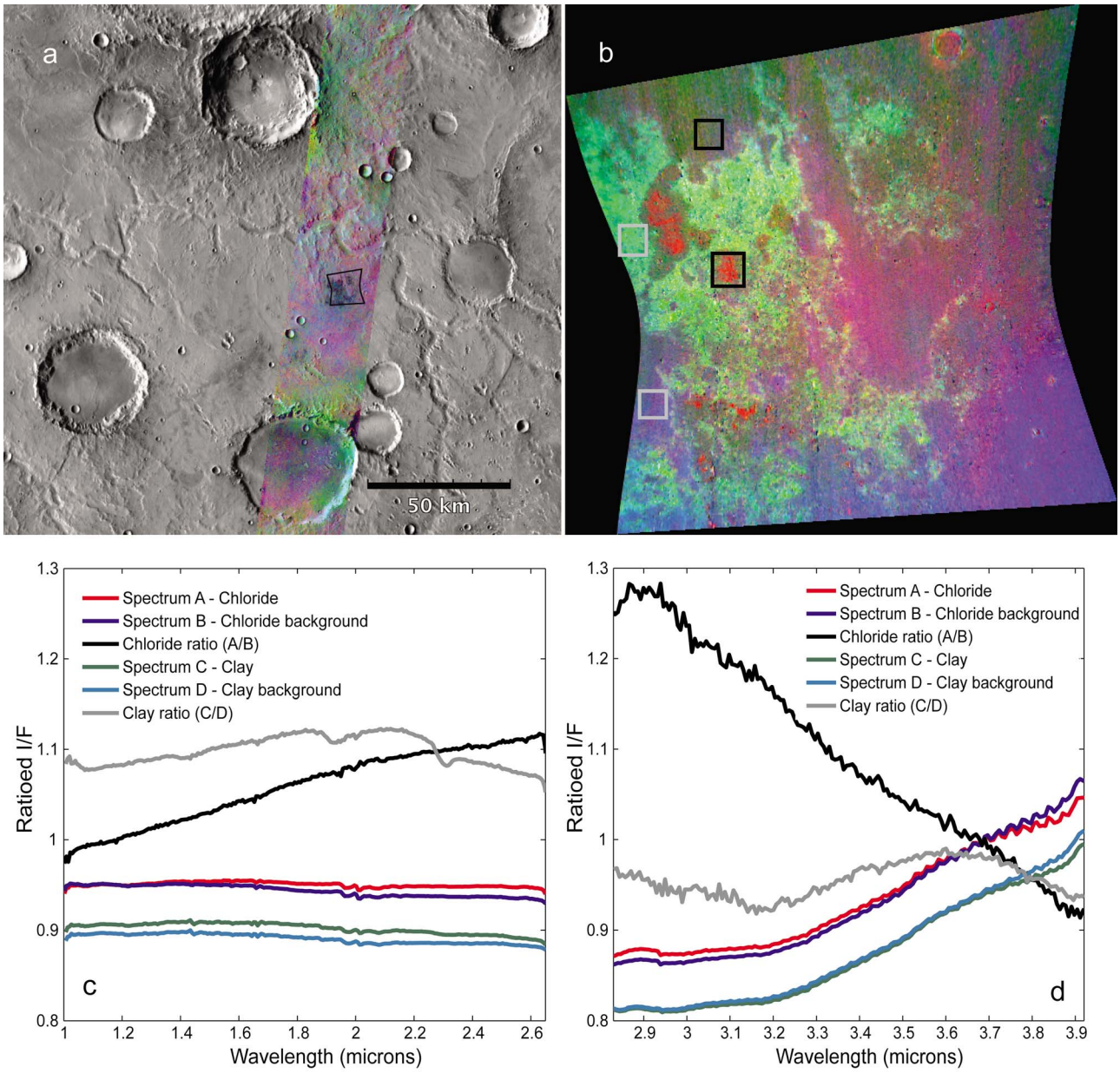


**Figure 2.** CRISM images depicting phyllosilicate-bearing and chloride-bearing regions, along with their characteristic NIR spectra. (a) THEMIS daytime IR DCS (9, 6, 4) image I01835005 showing the location of the CRISM image FRT00009ACE overlain onto the THEMIS daytime IR map. Image is centered at 353.5°E, −5.5°N. (b) CRISM color composite image of FRT00009ACE where red, green, and blue correspond to the reverse of the ISLOPE1, D2300 (2.3 $\mu$m drop off), and LCPINDEX parameters, respectively [*Pelkey et al.*, 2007]. Chlorides appear red, and phyllosilicates appear green. The image is ∼10 km across. Black boxes indicate the location of pixels averaged for the chloride-bearing region, and background spectra and gray boxes indicate the location of pixels averaged for the phyllosilicate-bearing region and background spectra in Figures 2c and 2d. (c) Characteristic CRISM ratio spectra of chloride-bearing units with a proximal phyllosilicate-bearing unit for comparison along with the raw numerator- and denominator-averaged spectra in the 1.1–2.5 $\mu$m wavelength range. (d) Characteristic CRISM ratioed and raw spectra in the 2.8–3.92 $\mu$m wavelength range. The chloride ratio spectrum indicates that the chloride units are more desiccated than the nearby pyroxene-bearing pixels averaged and used as the denominator spectrum.

*Fleischer et al.*, 2010]. The Spirit rover's Mössbauer data suggest the possible presence of pyrite or marcasite in a loose rock located atop the Home Plate outcrop named Fuzzy Smith [*Squyres et al.*, 2007; *Morris et al.*, 2008]. The detection is based on the presence of the Fe?D1 doublet in the Mössbauer data which is from either low-spin $Fe^{2+}$,

**Table 1.** Prepared Size Fractions for Materials Used in This Study

| Mineral/Rock | ≤10 μm | 63–90 μm | 125–180 μm | 180–250 μm | 250–355 μm |
|---|---|---|---|---|---|
| Labradorite | X | X | X | X | |
| Flood basalt | X | X | X | | X |
| Halite | X | X | X | X | X |
| Acid-washed pyrite | X | X | | | |

indicating $FeS_2$, or tetrahedral (tet)-$Fe^{3+}$, possibly a phyllosilicate [*Squyres et al.*, 2007; *Morris et al.*, 2008]. Fuzzy Smith has an unusual chemical composition that has not been observed by either rover; high Zn, the highest Si, K, and Ge measured at Gusev crater, and very low Ca and Fe [*Squyres et al.*, 2007]. The chemical and mineralogical data for Home Plate suggest a volcanic origin for Fuzzy Smith [*Squyres et al.*, 2007].

[13] The Wet Chemistry Laboratory (WCL) on NASA's Phoenix Mars Lander reported soluble sulfate equivalent to ~1.3 (±0.5) wt % as $SO_4$ in the soil around the lander, probably as $CaSO_4$ and/or $MgSO_4$ [*Kounaves et al.*, 2010]. Another result from the Phoenix lander's WCL is a sulfur (as $SO4^{2+}$) to total chloride ($Cl^-$ and $ClO_4^-$) ratio of ~2:1 [*Kounaves et al.*, 2010]. This is quite different from the relatively constant S/Cl ratio of ~4:1 observed by previous XRF. *Kounaves et al.* [2010] explained that this discrepancy may be due to soils in this region being chemically different than those observed by other rover/landers or some of the sulfur collected by the WCL was not/sparingly soluble.

#### 2.2.4. Martian Sulfide Geochemistry

[14] The presence of widespread sulfates on the surface of Mars observed both in situ by rovers/landers and by remote sensing instruments leads to questions about their source(s). *Burns and Fisher* [1993] hypothesized that percolating water containing oxidants (dissolved oxygen and $Fe^{3+}$) from photolysis of water vapor could initiate a set of reactions to form clays, sulfates and iron oxyhydroxides. Another hypothesis, based on laboratory simulations, is that sulfates could be produced by regional heating releasing sulfide-rich hydrothermal waters from the subsurface resulting in near-surface oxidation of pyrite-rich deposits [*Zolotov and Shock*, 2005]. A series of weathering experiments using metallic iron (α-Fe), magnetite, and pyrrhotite under simulated Martian conditions resulted in the production of elemental sulfur, sulfates, goethite and siderite in the case of metallic iron and iron sulfide [*Chevrier et al.*, 2004]. The extensive observation of sulfates and other oxidation products, as well as the lack of crustal recycling by plate tectonics on Mars suggests that sulfide deposits on the Martian surface are not likely to persist over geologic timescales.

## 3. Data, Samples, and Methods

[15] CRISM FRT and HRL data were analyzed for regions that displayed putative chloride salt deposits in THEMIS daytime infrared DCS images, with confirmed spectral character from extracted atmospherically corrected THEMIS emissivity spectra from the images. CRISM color composite images were made using CRISM summary products [*Pelkey et al.*, 2007; *Murchie et al.*, 2009]. In some regions, putative chloride salts are in close association with phyllosilicates [*Glotch et al.*, 2010]. To display phyllosilicates in association with the chloride deposits, red, green and blue were assigned to the inverse of the IR spectral slope parameter (chloride), D2300 (2.3 μm dropoff, phyllosilicate), and LCPINDEX (low-calcium pyroxene), respectively (Figure 2b). The volcano-scan correction technique was used to remove atmospheric absorptions present in the CRISM I/F data [*McGuire et al.*, 2009]. Spectra were extracted from atmospherically corrected CRISM hyperspectral image cubes by averaging pixels over areas bearing chloride (red) and phyllosilicate (green) signatures. In order to remove remnant atmospheric effects and instrumental calibration artifacts, spectra were then ratioed to regions in the image that were considered to be spectrally neutral (Figure 2c). In this case, pyroxene-bearing areas were used since dusty regions (which are generally spectrally neutral) within the images were absent.

### 3.1. Sample Description

[16] Natural samples of flood basalt, labradorite, and pyrite were obtained from Ward's Natural Science, and halite was acquired from Acros Organics (reagent grade 99%+ synthetic sodium chloride). Labradorite and flood basalt were chosen for use in this study due to the lack of strong absorptions within the spectral range. Labradorite mixtures and crusts represent a simple single mineral example and flood basalt mixtures and crusts represent a more realistic rock composition for comparison with the Martian surface. Halite was chosen as the chloride mineral used in this study due to its availability and relative stability in comparison with $MgCl_2$ and other anhydrous chlorides. Acid-washed pyrite was chosen due to its availability, and is assumed to be a proxy for other unoxidized Fe-sulfides. NIR spectra of many natural Fe sulfides have an absorption at ~1 μm due to the $Fe^{2+}$ crystal field band (Figure 1). This absorption can be due to either the $Fe^{2+}$ in the sulfide, an Fe oxide or hydroxide or another impurity phase.

[17] In order to achieve desired size fractions, flood basalt and labradorite were crushed in a tool steel mortar and pestle, halite was ground in an agate mortar and pestle and pyrite was ground using an automated agate ball mill. All ground samples were then dry sieved to several grain size fractions (Table 1). Particles of ≤10 μm grain size were separated using Stokes' settling method [*Day*, 1965; *Gee and Bauder*, 1986; *Salemi et al.*, 2010]. Settling was conducted at 22°C in a 600 mL beaker using HPLC (high-performance liquid chromatography) grade distilled water (ethanol was used for the settling of halite) and the supernatant containing the ≤10 μm size fraction was removed and placed into a beaker using a 100 mL glass pipette. After the sample had completely settled out of solution, excess water/ethanol was removed by pipette and the sample was dried in an 80°C oven (ethanol was removed through evaporation).

[18] Pyrite powders were acid washed with 1.0M deoxygenated HCl solution in a nitrogen environment for ≥ 30 min and subsequently rinsed with deoxygenated deionized water in a vacuum filtration system in a nitrogen glove box free of oxygen. Acid washing was necessary to ensure that oxidation products (primarily Fe sulfates and Fe oxide/hydroxides) were not present [e.g., *Karthe et al.*, 1993; *Elsetinow et al.*, 2003]. While in the nitrogen glove box, approximate masses of pyrite were weighed out and then transported in a sealed vial to the Vibrational Spectroscopy Laboratory (VSL) for precise

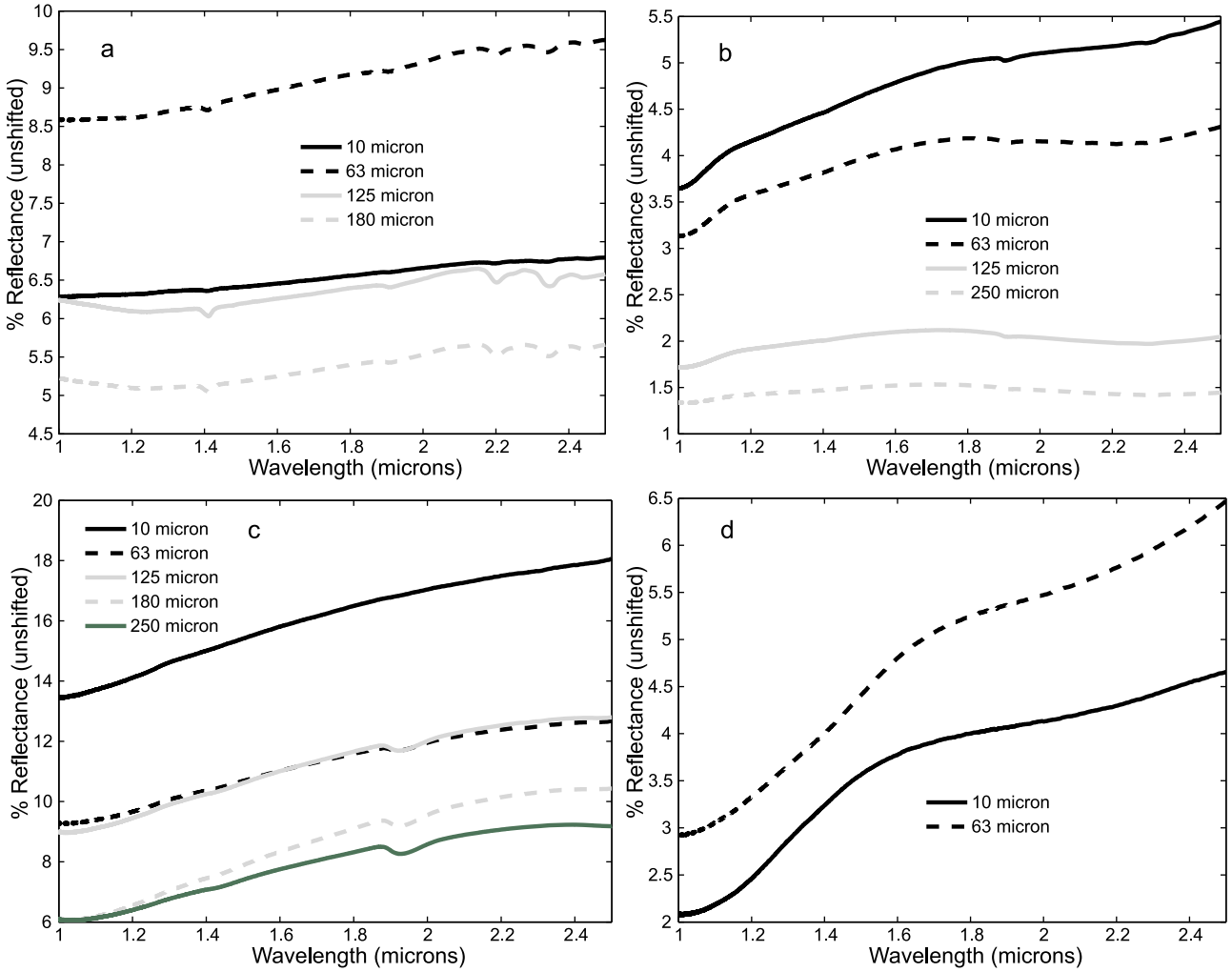


**Figure 3.** Diffuse reflectance spectra of (a) labradorite, (b) flood basalt, (c) halite, and (d) acid-washed pyrite for all grain sizes used in this study.

weight measurements prior to mixing. Accurate weight measurements could not be measured in the nitrogen glove box on the available balance. Great care was taken to ensure that the sample mixtures were not oxidized before spectral analysis.

[19] Diffuse reflectance spectra were collected from 1 to 2.5 $\mu$m for all grain sizes of the labradorite, flood basalt, halite and acid-washed pyrite used in this study (Table 1 and Figure 3). The spectra for labradorite slope upward toward longer wavelengths (red slope), with absorptions located at $\sim$1.4, 2.2, 2.35 and $\sim$2.45 $\mu$m due to a muscovite impurity and absorptions at $\sim$1.9 $\mu$m due to hydration of the samples (Figure 3a). The presence of muscovite is supported by the powder diffraction pattern of this sample (discussed below). Flood basalt powders display red sloping diffuse reflectance

**Table 2.** Halite Mixtures, Pyrite Mixtures, and Halite Crusts That Exhibit a Featureless Red Slope in NIR Ratio Spectra With Additional Absorptions Attributable to Either Hydration or Impurities[a]

| Mineral/Rock, Grain Size | 1% Halite | 5% Halite | 10% Halite | 25% Halite | 50% Halite | 75% Halite | Halite Crust | 25% Pyrite | 50% Pyrite |
|---|---|---|---|---|---|---|---|---|---|
| Flood basalt, $\leq$10 $\mu$m | | | | | | | | | |
| Flood basalt, 63–90 $\mu$m | X | X | X | X | | | | | |
| Flood basalt, 125–180 $\mu$m | X | X | X | X | | | X | | |
| Flood basalt, 250–355 $\mu$m | | | | | | | X | | |
| Labradorite, $\leq$10 $\mu$m | | | X | n.a. | X | X | X | | |
| Labradorite, 63–90 $\mu$m | X | X | X | n.a. | X | X | | | |
| Labradorite, 125–180 $\mu$m | X | X | X | n.a. | X | X | X | | |
| Labradorite, 180–250 $\mu$m | X | X | X | n.a. | X | X | X | | |

[a]Mixtures with halite were made with halite of the same size fraction as the labradorite or flood basalt. For acid-washed pyrite mixtures, $\leq$10 micron acid-washed pyrite was mixed with $\leq$10 micron labradorite and flood basalt, whereas 63–90 $\mu$m acid-washed pyrite was mixed with both 63–90 and 125–180 $\mu$m labradorite and flood basalt. Here, n.a., not applicable.

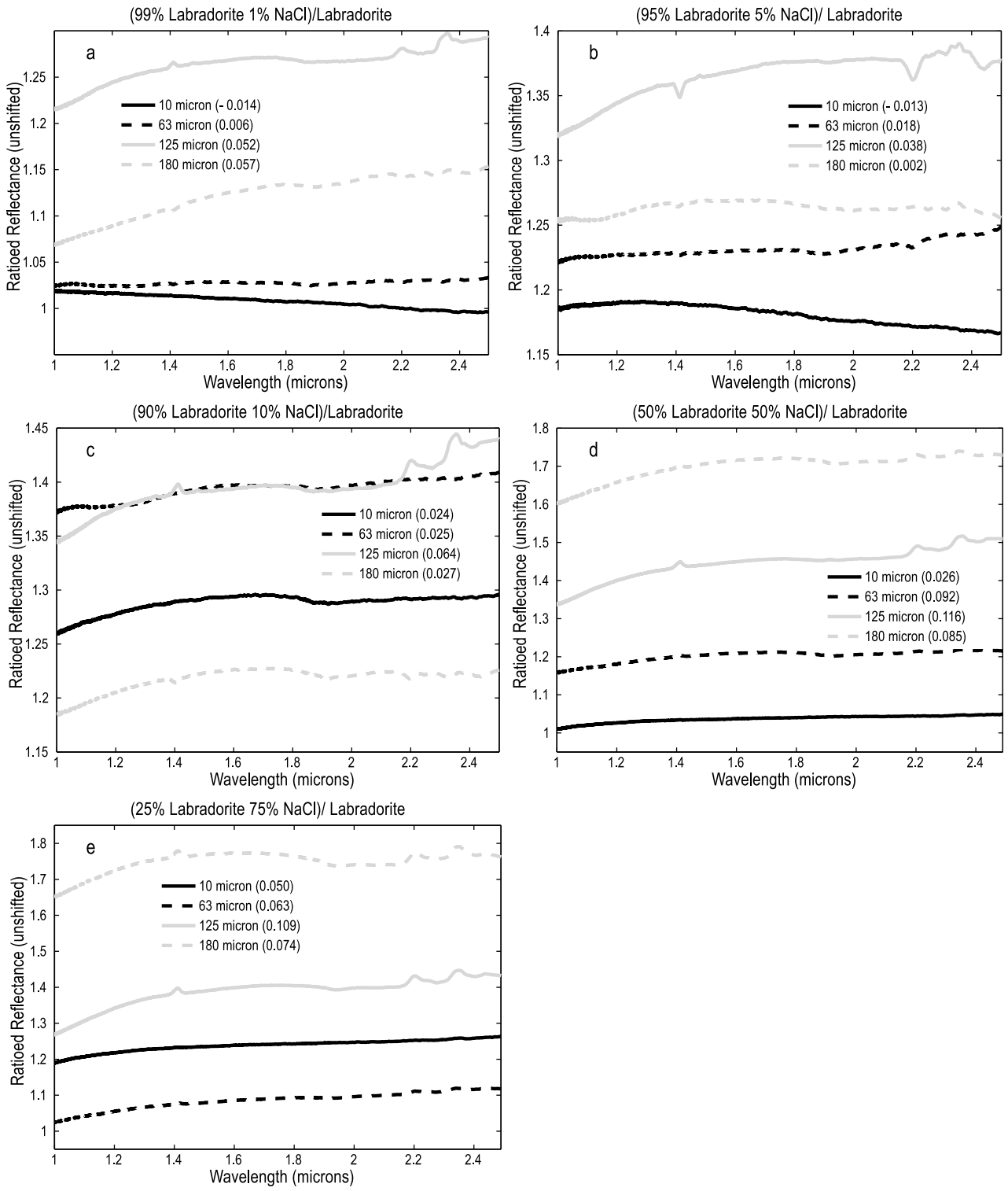


**Figure 4.** Ratio spectra for halite mixtures with labradorite with (a) 1 wt % halite, (b) 5 wt % halite, (c) 10 wt % halite, (d) 50 wt % halite, and (e) 75 wt % halite. Absorptions and negative absorptions located at 1.4, 2.2, 2.35, and ~2.45 $\mu$m are due to a muscovite impurity. The numbers in parentheses after the grain size labels in the legend indicate the spectral slope rounded to the nearest thousandths.

spectra, with absorptions located at ~1 and ~2.3 $\mu$m due to the presence of clinopyroxene and absorptions at ~1.9 $\mu$m due to hydration of the samples (Figure 3b). Halite samples reveal relatively featureless red sloping diffuse reflectance spectra with the only absorptions located at ~1.9 $\mu$m due to hydration (Figure 3c). Diffuse reflectance spectra of acid-washed pyrite also display red sloping spectra with broad absorptions located at ~1 and ~2 $\mu$m (Figure 3d). These

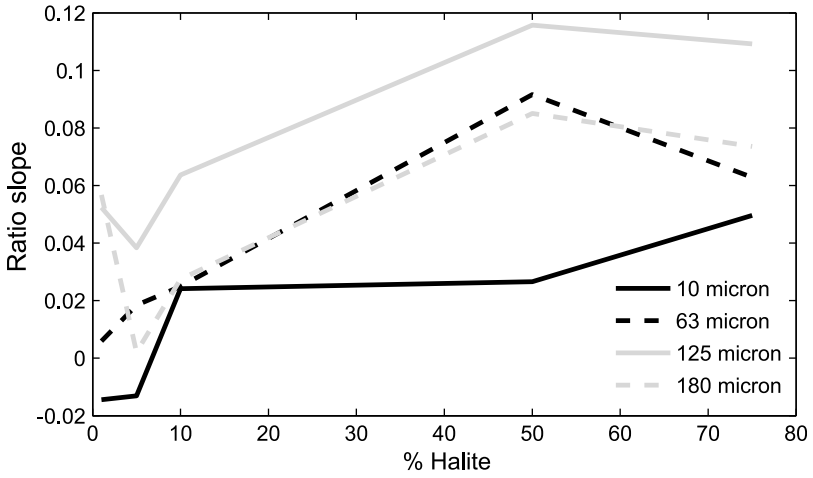


**Figure 5.** Plot of ratio spectral slope versus halite proportion for each grain size of labradorite.

absorptions in the acid-washed pyrite are due to either the incomplete removal of oxidation products in the acid washing process, oxidation of the pyrite in the time that it was exposed to ambient air or the natural spectral character of pyrite itself. It should be noted that the presence of slopes in these diffuse reflectance spectra are likely due to the use of a first surface gold mirror instead of MgO or spectralon as a reflectance standard. Since spectral ratios are used in this study for comparison to CRISM ratio spectra, the choice of reflectance standard does not affect the results.

[20] Powder diffraction patterns were collected to assess sample purity on a Rigaku Ultima IV X-ray diffractometer using Cu k$\alpha_{1,2}$ radiation, a DteX LPSD detector, 2.5 degree soller slits and a 0.01 degree step size. Data were collected at a rate of 0.5 degree $2\theta$ per minute. The powder diffraction patterns for the halite (10–120 degrees $2\theta$) and pyrite (20–110 degrees $2\theta$) samples reveal no impurities. The labradorite diffraction pattern (5–90 degrees $2\theta$) matches that of a sample from Labrador, Canada described as An52 and contains impurities that make up only a few wt % of the sample. These impurity phases include a K-rich feldspar (likely orthoclase), kaolinite and muscovite. The flood basalt powder diffraction pattern (10–90 degrees $2\theta$) reveals a composition of major plagioclase and minor clinopyroxene. Based on lattice parameters, the plagioclase phase in the flood basalt is about An50 or less. The clinopyroxene phase in the flood basalt is of space group C2/c indicating that it is in the range of diopside, augite, and hedenbergite. The clinopyroxene peaks in the flood basalt diffraction pattern are broadened, possibly indicating chemical inhomogeneity.

### 3.2. Halite and Pyrite Mixtures

[21] Silicate samples with the grain fractions listed in Table 1 were mixed with halite in proportions of 1, 10, 50 and 75 wt % halite. Additionally, Flood basalt mixtures with halite were also made with 25 wt % halite. Samples were gently mixed to obtain sample homogeneity and maintain grain size. These mixtures were then placed in a vacuum oven at 150°C for $\geq$ 5 days to remove surface-adsorbed water. Upon removal from the oven, samples were stored in a desiccator cabinet prior to spectral analysis.

[22] We also prepared 25 and 50 wt % mixtures using the acid-washed pyrite. Since only the $\leq$10 and 63–90 $\mu$m acid-washed pyrite size fractions were available, mixtures were only made using the $\leq$10, 63–90 and 125–180 $\mu$m grain sizes of the mixture rock and minerals. The comparatively larger density and smaller grain size of the pyrite resulted in heterogeneous mixing for larger size fractions.

[23] In addition to the particulate mixtures described above, we created a series of salt-crusted samples. Flood basalt and labradorite were added to sample vessels until they were two-thirds full (about 0.3 g) and then topped off with a saturated halite solution made with HPLC grade distilled water. These vessels were then stored in a desiccator for >3 days to evaporate the water and form a crust on the sample surface. If necessary, additional halite saturated solution was added followed by desiccation to form a relatively smooth surface for NIR analysis.

### 3.3. Visible and Near-Infrared Reflectance Measurements

[24] The dried sample mixtures were placed into a sample cup and diffuse near-infrared (0.8–2.5 $\mu$m) reflectance spectra were collected on the Stony Brook University Vibrational Spectroscopy Laboratory's Nicolet 6700 FTIR spectrometer equipped with a diffuse reflectance attachment, a $CaF_2$ beamsplitter and an uncooled InGaAs detector. For each sample, 1024 scans were recorded in the NIR spectral range using a white light source and a spectral resolution of 4 $cm^{-1}$. Spectra of the mixtures where then ratioed to spectra of pure labradorite or flood basalt of the same grain size to facilitate direct comparison to CRISM ratio spectra. A first surface gold mirror was used as a standard reference.

## 4. Laboratory Results

[25] Table 2 summarizes the results of the laboratory work, indicating which samples produced featureless red slopes in ratio spectra.

### 4.1. Halite Mixtures

#### 4.1.1. Mixtures With Labradorite

[26] Halite mixtures with labradorite result in red slopes in spectral ratios of the mixtures to pure labradorite for almost all samples, with a few exceptions (Figure 4). The $\leq$10 $\mu$m mixtures with halite proportions of 1 and 5 wt % result in a

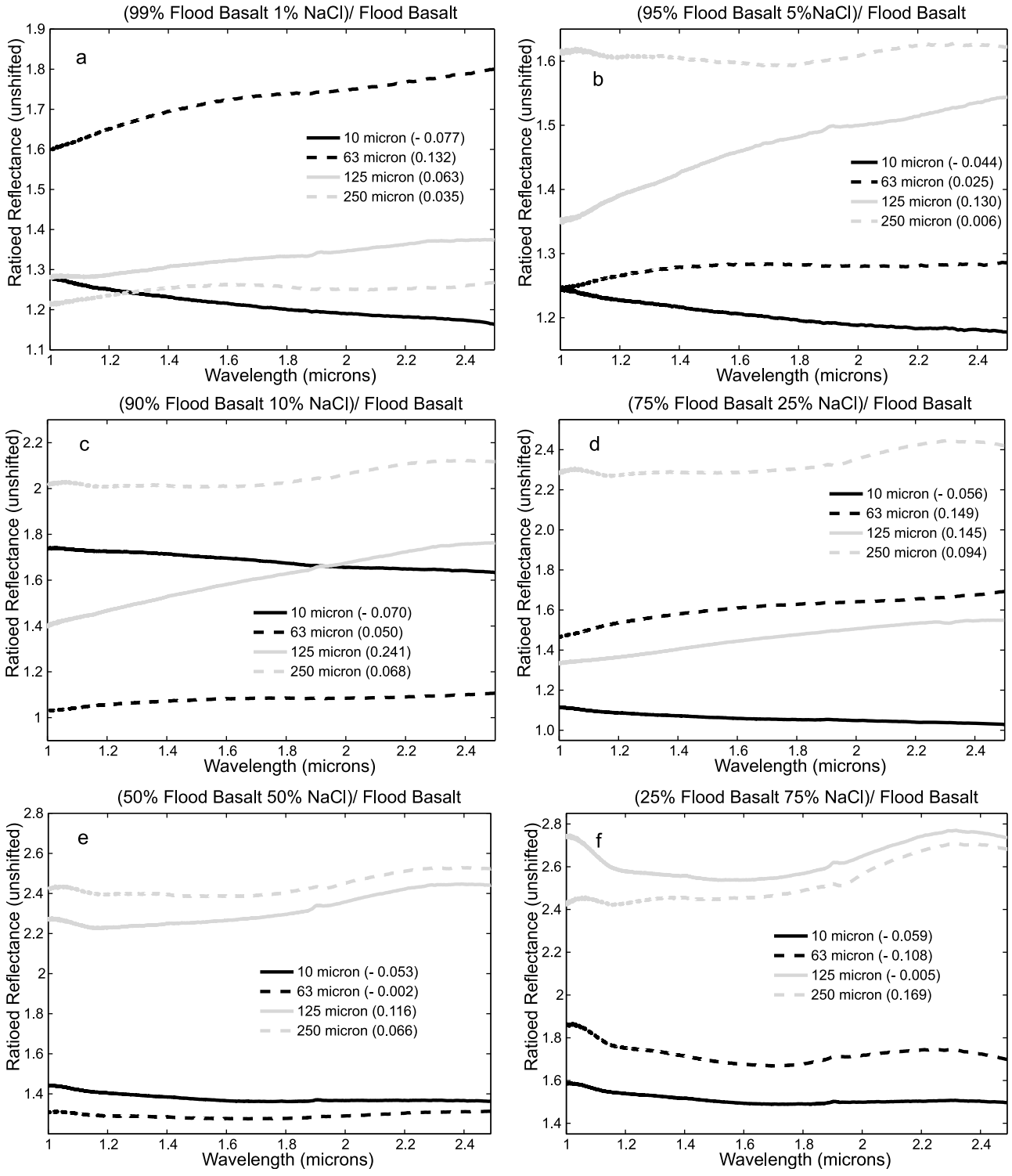


**Figure 6.** Ratio spectra for halite mixtures with flood basalt with (a) 1 wt % halite, (b) 5 wt % halite, (c) 10 wt % halite, (d) 25 wt % halite, (e) 50 wt % halite, and (f) 75 wt % halite. The numbers in parentheses after the grain size labels in the legend indicate the spectral slope rounded to the nearest thousandths.

blue featureless slope. The 180 $\mu$m grain size 5 wt % halite mixture results in a flat spectrum, with no overall slope. The presence of a muscovite impurity in the labradorite used in these experiments can be observed throughout the halite mixtures with labradorite. This impurity can be observed in the ratioed spectra as absorptions and ratio reflectance maxima at 1.4 $\mu$m, corresponding to overtones of the OH stretching modes, as well as at 2.2, 2.35 and $\sim$2.45 $\mu$m, corresponding to the metal-OH combination stretching plus bending vibrational bands. In many of the ratio spectra, and particularly noticeable in the 50 wt % mixtures, there is a broad hump between 1.4 and 1.9 $\mu$m that may be induced by

the absorptions attributable to the muscovite impurity. A general trend is observed that with increasing halite proportion, the slope of the ratio spectra is generally reddened for mixtures of all grain sizes (Figure 5). In summary, from 1 wt % to 75 wt % halite mixtures, a red slope is maintained in the ratio spectra with other absorptions attributed to the muscovite impurity in the labradorite, with a few noted exceptions.

#### 4.1.2. Mixtures With Flood Basalt

[27] Spectral ratios of halite mixtures with flood basalt to pure flood basalt spectra are shown in Figure 6. Halite mixtures of grain sizes of ≥ 63 $\mu$m, with 1–25 wt % halite result in an increase in reflectance with increasing wavelength observed in ratioed reflectance. At 75 wt % halite and above, a red slope is not clearly observed and a broad absorption is present in the ratio spectra between 1.2 and 2 $\mu$m due to the inversion of the flood basalt's clinopyroxene absorptions at ∼1 and 2.3 $\mu$m (Figure 6f). For the 50 wt % halite mixture of 63–90 $\mu$m grain size, the red slope is negligible and the 75 wt % halite mixture has a blue slope. The 250–355 $\mu$m ratio spectra for all halite proportions except 1 wt % clearly display an inversion of the clinopyroxene absorptions of the flood basalt. The ≤10 $\mu$m grain size mixtures for all proportions of halite display a blue slope. Hydration of the halite mixture with respect to the pure flood basalt can be observed in the ratio spectra as an absorption at 1.9 $\mu$m, corresponding to combination tones of the fundamental bending and stretching vibrations of $H_2O$. A ratio reflectance maximum at this wavelength results from the flood basalt sample being more hydrated with respect to the halite mixture. Figure 7 displays the relationship between ratio spectral slope and halite proportion for each grain size mixture with flood basalt.

### 4.2. Halite Crusts

#### 4.2.1. Labradorite Salt Crusts

[28] In the spectra of the 125–180 and 180–250 $\mu$m size fractions, absorptions result from the muscovite impurity in the labradorite sample, but the overall character of the spectral ratio is a red slope (Figure 8). A larger overall ratio reflectance value can be observed in the 125–180 $\mu$m halite crust sample due to the salt crust having a higher overall reflectance than the labradorite sample used as the denominator. The ≤10 $\mu$m grain size labradorite with halite crust sample also results in a slight red slope. The 63–90 $\mu$m grain size labradorite with halite crust samples result in a slightly blue sloped spectrum when ratioed to a pure labradorite of the same grain size. An absorption located at 1.9 $\mu$m is due to the presence of water not fully removed in the desiccation process of the saturated halite solution used to produce the salt crusts. As was observed in many of the halite/labradorite mixtures, a hump between 1.4 and 1.9 $\mu$m, particularly in the ≤10 and 125–180 $\mu$m labradorite with halite crust samples, can be seen that is likely caused by absorptions associated with the muscovite impurity in the labradorite.

#### 4.2.2. Flood Basalt Salt Crusts

[29] The two larger size fractions of flood basalt, 125–180 and 250–355 $\mu$m, resulted in salt crust spectra that produce red slopes when ratioed to pure flood basalt of the same grain size (Figure 9). The two smaller size fractions, ≤10 and 63–90 $\mu$m, resulted in ratio spectra that sloped downward toward longer wavelengths. The increased ratioed reflectance of the 250–355 $\mu$m sample is due to the larger overall reflectance of the halite crust spectrum with respect to the pure flood basalt spectrum used to produce the ratio. The absorption at 1.4 $\mu$m in the ≤10 and 250–355 $\mu$m grain size samples and at 1.9 $\mu$m in all flood basalt crust samples results from remnant water due to incomplete desiccation of the crust samples.

### 4.3. Pyrite Mixtures

#### 4.3.1. Mixtures With Labradorite

[30] The ratioed reflectance spectra of the 25 and 50 wt % pyrite mixtures with labradorite can be seen in Figures 10a and 10b, respectively. The ratio spectra of both the 25 and 50 wt % pyrite mixtures with labradorite to the labradorite standard include a red slope with a broad hump centered at ∼1.7 $\mu$m for all grain sizes. The 50 wt % pyrite, 125–180 $\mu$m grain size ratio spectrum lacks a slope, but still has the broad 1.7 $\mu$m feature. A simple relationship of increasing pyrite proportion resulting in increased slope toward longer wavelengths is observed. Reflectance maxima at 1.4, 2.2, 2.35 and ∼2.45 $\mu$m again correspond to the presence of muscovite in labradorite. The absorptions at ∼1 and 2.2 $\mu$m, producing the hump in the spectral ratios at ∼1.7 $\mu$m, results from either the $Fe^{2+}$ crystal field absorptions due to pyrite itself or the presence of pyrite oxidation products in the form of either Fe oxides or oxyhydroxides. The presence of oxidation products results from their incomplete removal in the acid washing process and/or oxidation from exposure to ambient air in the time period required for sample mixing and preparation for data collection [*Karthe et al.*, 1993; *Swayze et al.*, 2000]. If the pyrite mixtures are allowed to sit in ambient air for longer time periods, the observed broad spectral maximum grows in size. This is especially noticeable in the ≤10 $\mu$m size fractions resulting from the extended time period necessary to gently mix and achieve homogeneity of the pyrite and labradorite using a mortar and pestle.

#### 4.3.2. Mixtures With Flood Basalt

[31] In ratioed reflectance spectra, mixtures of 25 and 50 wt % pyrite resulted in a red slope for all three grain sizes used in this study (Figure 11). Excluding the 63–90 $\mu$m mixtures, a trend of steepening red slope with increasing pyrite fraction is observed. A noticeable broad hump centered at around 1.6 $\mu$m, especially in the ≤10 $\mu$m size fraction, likely results from the presence of oxidation products in the pyrite, specifically Fe oxides and hydroxides [*Karthe et al.*, 1993; *Swayze et al.*, 2000]. A reflectance maximum at 1.9 $\mu$m is produced in all ratio spectra, apart from the 50 wt % pyrite mixture of 63–90 $\mu$m particle size, due to hydration of the flood basalt used as the denominator of the spectral ratio with respect to the pyrite mixtures.

## 5. Discussion

[32] Some halite mixtures with labradorite or flood basalt were effective in emulating the featureless red slope previously observed in CRISM data for putative chloride deposits [*Wray et al.*, 2009; *Murchie et al.*, 2009; *Glotch et al.*, 2010]. After accounting for the muscovite impurity present in the labradorite used in this study, all halite proportions mixed with labradorite successfully imitate the NIR remote sensing spectral character, excluding the 1 wt % and 5 wt % halite mixtures of ≤10 $\mu$m grain size. A hump in many of the

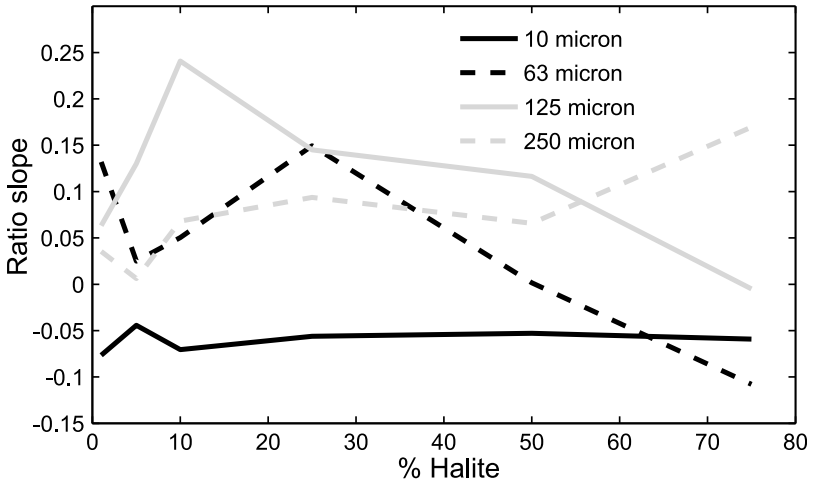


**Figure 7.** Plot of ratio spectral slope versus halite proportion for each grain size of flood basalt.

labradorite ratio spectra between 1.4 and 1.9 $\mu$m, believed to be associated with the presence of muscovite, is observed mainly in the 180 $\mu$m mixtures but dominates in 10 wt % halite spectra of all grain sizes. Fewer flood basalt mixtures are successful in emulating the CRISM ratio spectra. Mixtures composed of 1–25 wt % halite reveal a featureless red slope for particle sizes of 63–90 and 125–180 $\mu$m, other than a hydration feature at 1.9 $\mu$m present in many of the ratio spectra. Halite crusts on labradorite emulated a featureless red slope for all but the 63–90 $\mu$m grain size fraction, whereas halite crusts on flood basalt were only successful for 125–180 and 250–355 $\mu$m grain sizes.

[33] Average thermal inertia values derived for these proposed chloride-bearing units from THEMIS data are >350 $Jm^{-2}K^{-1}s^{-1/2}$, indicating grain sizes greater than ~900 $\mu$m or indurated materials [*Presley and Christensen*, 1997; *Mellon et al.*, 2000; *Putzig et al.*, 2005; *Osterloo et al.*, 2010]. For labradorite mixtures composed of 1–5 wt % halite, the ≤10 $\mu$m grain size is incapable of producing a red slope whereas larger size fractions are successful. However, for larger halite proportions, even the ≤10 $\mu$m particle size was capable of emulating the featureless red slope found for these deposits in CRISM data. The largest grain size used in the halite-flood basalt mixtures was unable to emulate the CRISM spectral behavior. Halite crusts on both labradorite and flood basalt produced red slopes only for the for larger grain sizes, consistent with the suggestion from thermal inertia measurements [*Osterloo et al.*, 2010], that the Martian deposits may be indurated.

[34] Halite crusts would be more likely to be formed initially on the Martian surface via groundwater upwelling or pooling of brines on the surface. Late Noachian to early Hesperian crater count-based age estimates for Martian chloride deposits would indicate that these deposits have

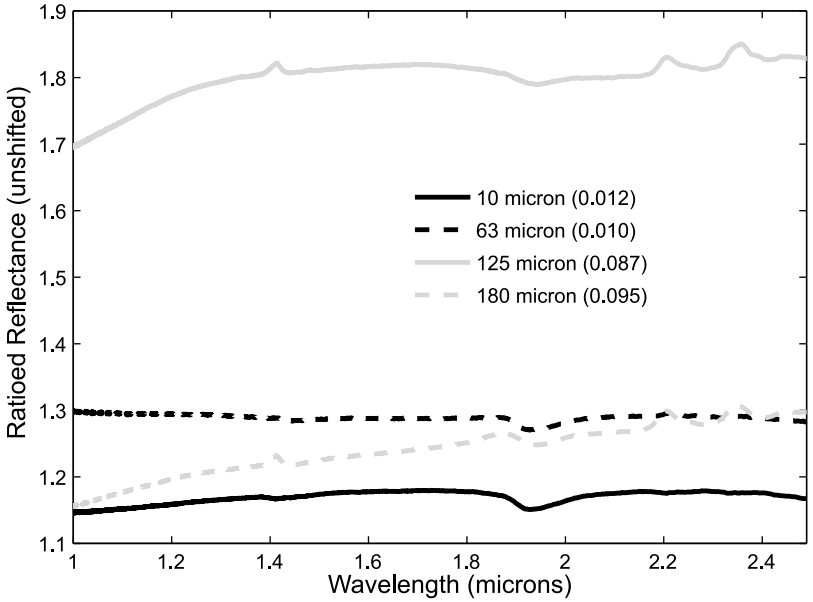


**Figure 8.** Ratio spectra for halite crusts on labradorite of given size fractions. The numbers in parentheses after the grain size labels in the legend indicate the spectral slope rounded to the nearest thousandths.

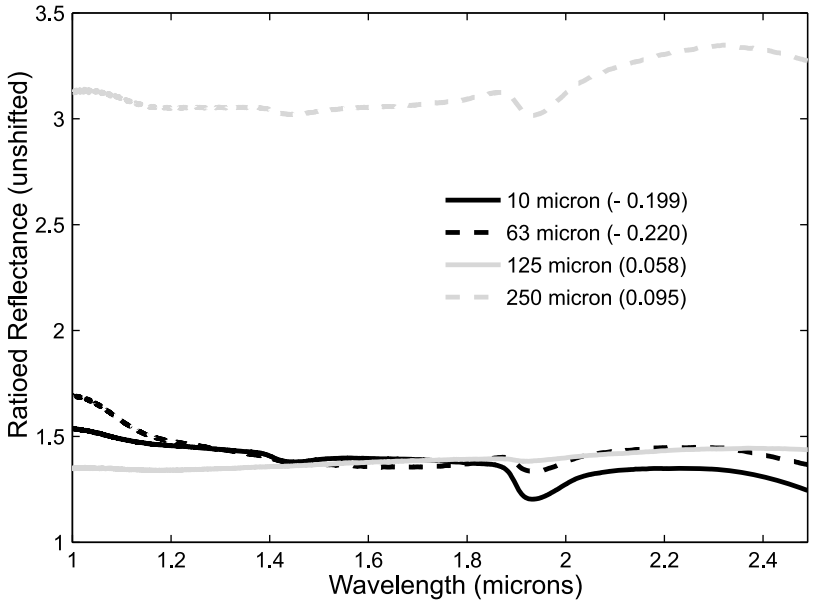


**Figure 9.** Ratio spectra for halite crusts on flood basalt of given size fractions. The numbers in parentheses after the grain size labels in the legend indicate the spectral slope rounded to the nearest thousandths.

been exposed to the atmosphere and aeolian processes for ~3.5 Gy or more [*Osterloo et al.*, 2010]. Formation of intimate mixtures, like those in this study, could be produced by extensive aeolian mixing of chloride in the form of surficial crusts with surrounding basaltic materials.

[35] Pyrite mixtures were not capable of imitating the spectral shape observed in the CRISM data for proposed chloride units on the Martian surface. A large hump centered between 1.6 and 1.7 $\mu$m, due to rapid oxidation forming Fe-oxides and hydroxides during the sample preparation and data collection time (generally <15 min), dominates all pyrite mixture data for both flood basalt and labradorite. Based on the extensive presence of sulfates as well as Fe oxides and hydroxides across the Martian surface observed by both NIR remote sensing instruments and lander/rover data, pyrite would not persist without extensive oxidation. The age of the deposits calculated from crater counting indicates that these units range from late Hesperian to early Noachian (2.6–4.1 Gy) [*Tanaka*, 1986; *Tanaka and Hartmann*, 2008; *Osterloo et al.*, 2010]. We conclude that the presence chloride salts is indeed the most likely explanation for these spectrally anomalous units in the Martian southern highlands.

[36] The data we acquired for this study do not allow us to place tight constraints on the abundance of chloride in Martian deposits. The flood basalt results are important since the composition of the Martian crust in the regions where these deposits are observed is mainly Surface Type 1 or Group 2 from TES data [*Bandfield et al.*, 2000; *Rogers and*

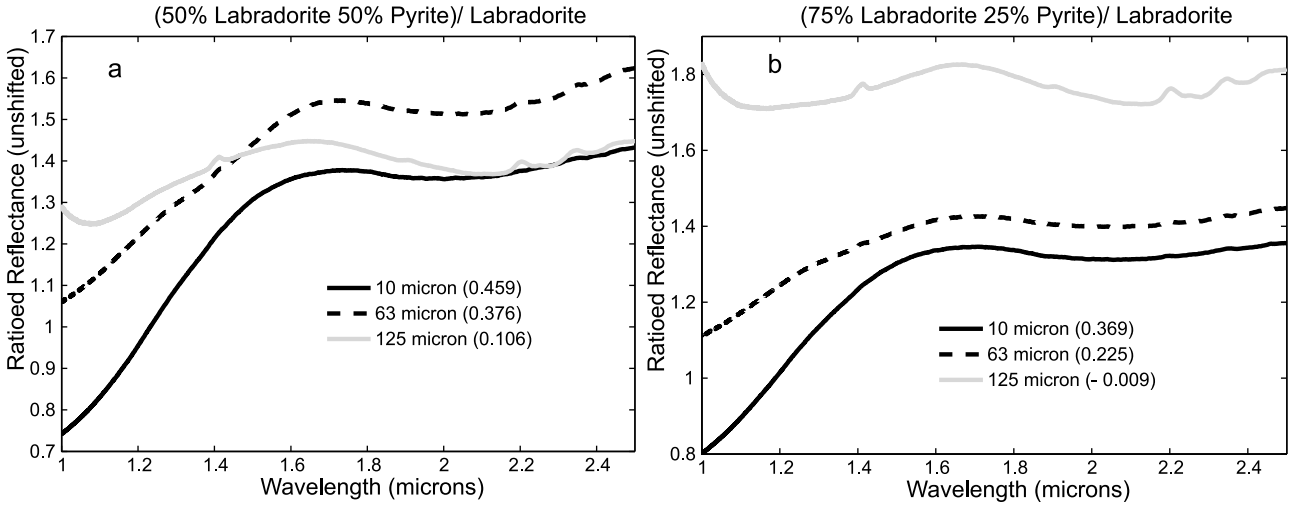


**Figure 10.** Spectral ratios for mixtures of labradorite with (a) 50 wt % pyrite and (b) 25 wt % pyrite. The numbers in parentheses after the grain size labels in the legend indicate the spectral slope rounded to the nearest thousandths.

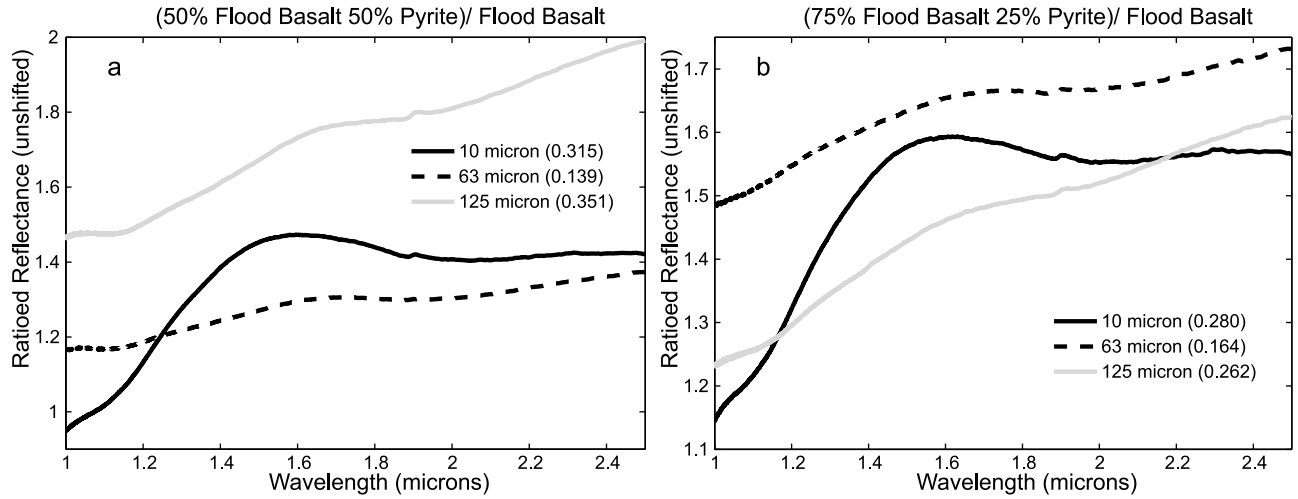


**Figure 11.** Spectral ratios for mixtures of flood basalt with (a) 50 wt % pyrite and (b) 25 wt % pyrite. The numbers in parentheses after the grain size labels in the legend indicate the spectral slope rounded to the nearest thousandths.

*Christensen*, 2007]. Surface Type 1 is compositionally similar to terrestrial basalt/ low-Si basaltic andesite containing ~65 vol. % plagioclase and ~30 vol. % clinopyroxene with 45–57 wt % $SiO_2$ [*Bandfield et al.*, 2000]. Group 2 is defined by the Syrtis TES spectral shape with a derived modal mineralogy of 31% plagioclase, 29% high-Ca clinopyroxene, 12% high-Si phases, 7% olivine, 4% orthopyroxene and 17% other (carbonate, sulfate, amphibole, quartz, and alkali-feldspar) [*Rogers and Christensen*, 2007]. Whereas the success of labradorite mixtures was not influenced by halite proportion and only the 1 and 5 wt % halite mixtures of ≤10 $\mu$m grain size were unable to produce the desired spectral character, flood basalt mixtures were more conditionally successful in this study. Flood basalt mixtures of ≤25 wt % halite and grain sizes between 63 and 180 $\mu$m were most effective in producing featureless red slopes in ratio spectra. This is the tightest constraint of possible composition and grain size of these deposits that can be concluded from this NIR study. Slopes produced in ratio spectra from this laboratory study are not quantitatively compared with CRISM ratio spectra because the laboratory ratios were formed using raw diffuse reflectance spectra and the CRISM ratio spectra are based on I/F data. Current studies being conducted in the mid-IR wavelength range of similar mixtures may be able to better constrain chloride abundance and effective grain size for these units.

## 6. Conclusions

[37] In an effort to reproduce the NIR spectral character of putative chloride deposits observed on Mars by the CRISM instrument, simple mixtures of multiple particle sizes were made of halite/pyrite with flood basalt and labradorite as substrates. Along with these simple mixtures, halite salt crusts were formed on the surfaces of flood basalt and labradorite of varying grain sizes.

[38] The halite mixtures and salt crusts proved to be successful in producing the desired spectral character in many cases. Other than the ≤10 $\mu$m size fraction mixtures with halite of the two smallest proportions, all of the labradorite mixtures produced red sloping spectra, with spectral features easily attributable to water associated with the halite or a muscovite impurity within the labradorite. The success of halite mixtures with flood basalt was more limited; proportions of >25 wt % halite resulted in spectral character inconsistent with the Martian deposits, and smaller proportions were only successful in the 63–90 and 125–180 $\mu$m grain sizes. The halite salt crusts on labradorite were also largely successful except for the 63–90 $\mu$m size fraction, whereas the flood basalt samples were only capable of emulating the desired spectral character in the case of the 125–180 and 250–355 $\mu$m size fractions.

[39] The pyrite mixtures with both labradorite and flood basalt were incapable of reproducing the spectral behavior observed in CRISM ratio spectra, regardless of grain size or proportion. This is due to the rapid appearance of oxidation products in the acid-washed pyrite from the ≤15 min of time spent in open air that is necessary to produce homogeneous mixtures and collect NIR data. At this point, it is possible to discount pyrite as a possible component of the Martian deposits. This can bring us to the conclusion that these units are chloride-bearing, even if the proportion cannot be tightly constrained by this study. We are currently conducting a mid-IR spectral study using similar mixtures in an effort to place further constraints on both grain size and chloride abundance.

[40] **Acknowledgments.** This work was funded in part by NASA Mars Data Analysis program grant NNX08AK93G made to T.D.G. We thank William R. Woerner for collecting and analyzing the powder diffraction patterns of the mineral and rock samples to assess purity. Use of the Rigaku diffractometer was supported by NASA grant MFRP07-0022, awarded to John B. Parise. We would also like to thank Martin A. A. Schoonen for the use of his lab and Alexander Smirnov for his assistance in the process of acid washing our pyrite powders. We thank Kim Seelos and an anonymous reviewer for detailed comments that improved the content and clarity of the original paper.

## References

Bandfield, J. L., V. E. Hamilton, and P. R. Christensen (2000), A global view of Martian surface compositions from MGS-TES, *Science*, *287*(5458), 1626–1630, doi:10.1126/science.287.5458.1626.

Bernard, A., and F. Le Guern (1986), Condensation of volatile elements in high-temperature gases of Mount St. Helens, *J. Volcanol. Geotherm. Res.*, *28*(1–2), 91–105, doi:10.1016/0377-0273(86)90007-7.

Bridges, J. C., and M. M. Grady (1999), A halite-siderite-anhydrite-chlorapatite assemblage in Nakhla: Mineralogical evidence for evaporites on Mars, *Meteorit. Planet. Sci.*, *34*(3), 407–415, doi:10.1111/j.1945-5100.1999.tb01349.x.

Bridges, J. C., and M. M. Grady (2000), Evaporite mineral assemblages in the nakhlite (Martian) meteorites, *Earth Planet. Sci. Lett.*, *176*(3–4), 267–279, doi:10.1016/S0012-821X(00)00019-4.

Bridges, J. C., D. C. Catling, J. M. Saxton, T. D. Swindle, I. C. Lyon, and M. M. Grady (2001), Alteration assemblages in Martian meteorites: Implications for near-surface processes, *Space Sci. Rev.*, *96*, 365–392, doi:10.1023/A:1011965826553.

Brückner, J., G. Dreibus, R. Rieder, and H. Wänke (2003), Refined data of Alpha Proton X-ray Spectrometer analyses of soils and rocks at the Mars Pathfinder site: Implications for surface chemistry, *J. Geophys. Res.*, *108*(E12), 8094, doi:10.1029/2003JE002060.

Burgess, R., I. P. Wright, and C. T. Pillinger (1989), Distribution of sulphides and oxidised sulphur components in SNC meteorites, *Earth Planet. Sci. Lett.*, *93*(3–4), 314–320, doi:10.1016/0012-821X(89)90030-7.

Burns, R. G., and D. S. Fisher (1990), Evolution of sulfide mineralization on Mars, *J. Geophys. Res.*, *95*(B9), 14,169–14,173, doi:10.1029/JB095iB09p14169.

Burns, R. G., and D. S. Fisher (1993), Rates of oxidative weathering on the surface of Mars, *J. Geophys. Res.*, *98*(E2), 3365–3372, doi:10.1029/92JE02055.

Chevrier, V., P. Rochette, P. E. Mathe, and O. Grauby (2004), Weathering of iron-rich phases in simulated Martian atmospheres, *Geology*, *32*(12), 1033–1036, doi:10.1130/G21078.1.

Clark, B. C., A. K. Baird, R. J. Weldon, D. M. Tsusaki, L. Schnabel, and M. P. Candelaria (1982), Chemical composition of Martian fines, *J. Geophys. Res.*, *87*(B12), 10,059–10,067, doi:10.1029/JB087iB12p10059.

Day, P. R. (1965), Particle fractionation and particle-size analysis, in *Methods of Soil Analysis, Part 1: Physical and Mineralogical Properties, Including Statistics of Measurement and Sampling*, edited by C. A. Black et al., pp. 545–567, Am. Soc. of Agron., Madison, Wis.

Deer, W. A., R. A. Howie, and J. Zussman (1992), *An Introduction to Rock-Forming Minerals*, 2nd ed., 696 pp., Pearson, Harlow, U. K.

Elsetinow, A. R., M. J. Borda, M. A. A. Schoonen, and D. R. Strongin (2003), Suppression of pyrite oxidation in acidic aqueous environments using lipids having two hydrophobic tails, *Adv. Environ. Res.*, *7*(4), 969–974, doi:10.1016/S1093-0191(02)00101-6.

Eugster, H. P., and L. A. Hardie (1978), Saline lakes, in *Lakes: Chemistry, Geology, Physics*, edited by A. Lerman, pp. 237–293, Springer, New York.

Fleischer, I., et al. (2010), Mineralogy and chemistry of cobbles at Meridiani Planum, Mars, investigated by the Mars Exploration Rover Opportunity, *J. Geophys. Res.*, *115*, E00F05, doi:10.1029/2010JE003621.

Gee, G. W., and J. W. Bauder (1986), Particle-size analysis, in *Methods of Soil Analysis, Part 1: Physical and Mineralogical Methods*, *Agron. Monogr.*, vol. 9, 2nd ed., edited by A. Klute, pp. 383–411, Am. Soc. of Agron., Madison, Wis.

Gellert, R., et al. (2006), Alpha particle X-ray spectrometer (APXS): Results from Gusev crater and calibration report, *J. Geophys. Res.*, *111*, E02S05, doi:10.1029/2005JE002555.

Gillespie, A. R., A. B. Kahle, and R. E. Walker (1986), Color enhancement of highly correlated images. I. Decorrelation and HSI contrast stretches, *Remote Sens. Environ.*, *20*(3), 209–235, doi:10.1016/0034-4257(86)90044-1.

Glotch, T. D., J. L. Bandfield, L. L. Tornabene, H. B. Jensen, and F. P. Seelos (2010), Distribution and formation of chlorides and phyllosilicates in Terra Sirenum, Mars, *Geophys. Res. Lett.*, *37*, L16202, doi:10.1029/2010GL044557.

Goodall, T. M., C. P. North, and K. W. Glennie (2000), Surface and subsurface sedimentary structures produced by salt crusts, *Sedimentology*, *47*(1), 99–118, doi:10.1046/j.1365-3091.2000.00279.x.

Gooding, J. L., K. E. Aggrey, and D. W. Muenow (1990), Volatile compounds in shergottite and nakhlite meteorites, *Meteoritics*, *25*, 281–289.

Gooding, J. L., S. J. Wentworth, and M. E. Zolensky (1991), Aqueous alteration of the Nakhla meteorite, *Meteoritics*, *26*(2), 135–143.

Guilbert, J. M., and C. F. J. Park (1986), *The Geology of Ore Deposits*, 985 pp., W. H. Freeman, New York.

Hardie, L. A., J. P. Smoot, and H. P. Eugster (1978), Saline lakes and their deposits: A sedimentological approach, in *Modern and Ancient Lake Sediments*, edited by A. Matter and M. E. Tucker, pp. 7–41, Blackwell, Oxford, U. K., doi:10.1002/9781444303698.ch2.

Hecht, M. H., et al. (2009), Detection of perchlorate and the soluble chemistry of Martian soil at the Phoenix lander site, *Science*, *325*(5936), 64–67, doi:10.1126/science.1172466.

Hem, J. D. (1992), Study and interpretation of the chemical characteristics of natural water, *U.S. Geol. Surv. Water Supply Pap.*, *2254*, 363 pp.

Hunt, G. R., J. W. Salisbury, and C. J. Lenhoff (1971), Visible and near-infrared spectra of minerals and rocks: IV. Sulphides and sulphates, *Mod. Geol.*, *3*, 1–14.

Hunt, G. R., J. W. Salisbury, and C. J. Lenhoff (1972), Visible and near-infrared spectra of minerals and rocks: V. Halides, arsenates, vanadates, and borates, *Mod. Geol.*, *3*, 121–132.

Jambor, J. L., D. K. Nordstrom, and C. N. Alpers (2000), Metal-sulfate salts from sulfide mineral oxidation, in *Sulfate Minerals: Crystallography, Geochemistry, and Environmental Significance*, edited by C. N. Alpers et al., pp. 303–350, Mineral. Soc. of Am., Washington, D. C.

Karthe, S., R. Szargan, and E. Suoninen (1993), Oxidation of pyrite surfaces: A photoelectron spectroscopic study, *Appl. Surf. Sci.*, *72*(2), 157–170, doi:10.1016/0169-4332(93)90007-X.

Kounaves, S. P., et al. (2010), Soluble sulfate in the Martian soil at the Phoenix landing site, *Geophys. Res. Lett.*, *37*, L09201, doi:10.1029/2010GL042613.

Lorand, J. P., V. Chevrier, and V. Sautter (2005), Sulfide mineralogy and redox conditions in some shergottites, *Meteorit. Planet. Sci.*, *40*(8), 1257–1272, doi:10.1111/j.1945-5100.2005.tb00187.x.

McGuire, P. C., et al. (2009), An improvement to the volcano-scan algorithm for atmospheric correction of CRISM and OMEGA spectral data, *Planet. Space Sci.*, *57*(7), 809–815, doi:10.1016/j.pss.2009.03.007.

McSween, H. Y., Jr. (1985), SNC meteorites: Clues to Martian petrologic evolution?, *Rev. Geophys.*, *23*(4), 391–416, doi:10.1029/RG023i004p00391.

Mellon, M. T., B. M. Jakosky, H. H. Kieffer, and P. R. Christensen (2000), High-resolution thermal inertia mapping from the Mars Global Surveyor Thermal Emission Spectrometer, *Icarus*, *148*(2), 437–455, doi:10.1006/icar.2000.6503.

Milliken, R. E., and D. L. Bish (2010), Sources and sinks of clay minerals on Mars, *Philos. Mag.*, *90*(17–18), 2293–2308, doi:10.1080/14786430903575132.

Ming, D. W., et al. (2008), Geochemical properties of rocks and soils in Gusev Crater, Mars: Results of the Alpha Particle X-Ray Spectrometer from Cumberland Ridge to Home Plate, *J. Geophys. Res.*, *113*, E12S39, doi:10.1029/2008JE003195.

Morris, R. V., et al. (2008), Iron mineralogy and aqueous alteration from Husband Hill through Home Plate at Gusev Crater, Mars: Results from the Mössbauer instrument on the Spirit Mars Exploration Rover, *J. Geophys. Res.*, *113*, E12S42, doi:10.1029/2008JE003201.

Murchie, S. L., et al. (2009), A synthesis of Martian aqueous mineralogy after 1 Mars year of observations from the Mars Reconnaissance Orbiter, *J. Geophys. Res.*, *114*, E00D06, doi:10.1029/2009JE003342.

Osterloo, M. M., V. E. Hamilton, J. L. Bandfield, T. D. Glotch, A. M. Baldridge, P. R. Christensen, L. L. Tornabene, and F. S. Anderson (2008), Chloride-bearing materials in the southern highlands of Mars, *Science*, *319*(5870), 1651–1654, doi:10.1126/science.1150690.

Osterloo, M. M., F. S. Anderson, V. E. Hamilton, and B. M. Hynek (2010), Geologic context of proposed chloride-bearing materials on Mars, *J. Geophys. Res.*, *115*, E10012, doi:10.1029/2010JE003613.

Pelkey, S. M., et al. (2007), CRISM multispectral summary products: Parameterizing mineral diversity on Mars from reflectance, *J. Geophys. Res.*, *112*, E08S14, doi:10.1029/2006JE002831.

Presley, M. A., and P. R. Christensen (1997), Thermal conductivity measurements of particulate materials: 2. Results, *J. Geophys. Res.*, *102*(E3), 6551–6566, doi:10.1029/96JE03303.

Putzig, N. E., M. T. Mellon, K. A. Kretke, and R. E. Arvidson (2005), Global thermal inertia and surface properties of Mars from the MGS mapping mission, *Icarus*, *173*(2), 325–341, doi:10.1016/j.icarus.2004.08.017.

Rieder, R., et al. (2004), Chemistry of rocks and soils at Meridiani Planum from the Alpha Particle X-ray Spectrometer, *Science*, *306*(5702), 1746–1749, doi:10.1126/science.1104358.

Rogers, A. D., and P. R. Christensen (2007), Surface mineralogy of Martian low-albedo regions from MGS-TES data: Implications for upper crustal evolution and surface alteration, *J. Geophys. Res.*, *112*, E01003, doi:10.1029/2006JE002727.

Salemi, E., U. Tessari, N. Colombani, and M. Mastrocicco (2010), Improved gravitational grain size separation method, *Appl. Clay Sci.*, *48*(4), 612–614, doi:10.1016/j.clay.2010.03.014.

Schröder, C., et al. (2008), Meteorites on Mars observed with the Mars Exploration Rovers, *J. Geophys. Res.*, *113*, E06S22, doi:10.1029/2007JE002990.

Schröder, C., et al. (2010), Properties and distribution of paired candidate stony meteorites at Meridiani Planum, Mars, *J. Geophys. Res.*, *115*, E00F09, doi:10.1029/2010JE003616.

Squyres, S. W., et al. (2007), Pyroclastic activity at Home Plate in Gusev Crater, Mars, *Science*, *316*(5825), 738–742, doi:10.1126/science.1139045.

Swayze, G. A., et al. (2000), Using imaging spectroscopy to map acidic mine waste, *Environ. Sci. Technol.*, *34*(1), 47–54, doi:10.1021/es990046w.

Symonds, R. B., W. I. Rose, M. H. Reed, F. E. Lichte, and D. L. Finnegan (1987), Volatilization, transport, and sublimation of metallic and non-metallic elements in high temperature gases at Merapi Volcano, Indonesia, *Geochim. Cosmochim. Acta*, *51*(8), 2083–2101, doi:10.1016/0016-7037(87)90258-4.

Tanaka, K. L. (1986), The stratigraphy of Mars, *Proc. Lunar Planet. Sci. Conf. 17th*, Part 1, *J. Geophys. Res.*, *91*, suppl., E139–E158, doi:10.1029/JB091iB13p0E139.

Tanaka, K. L., and W. K. Hartmann (2008), The planetary timescale, in *The Concise Geologic Time Scale*, edited by J. G. Ogg et al., pp. 13–22, Cambridge Univ. Press, New York.

Wentworth, S. J., K. L. Thomas-Keptra, and D. S. McKay (2000), Weathering and secondary minerals in the Martian meteorite Shergotty, *Lunar Planet Sci.*, *XXXI*, Abstract 1888.

Wray, J. J., S. L. Murchie, S. W. Squyres, F. P. Seelos, and L. L. Tornabene (2009), Diverse aqueous environments on ancient Mars revealed in the southern highlands, *Geology*, *37*(11), 1043–1046, doi:10.1130/G30331A.1.

Zolotov, M. Y., and E. L. Shock (2005), Formation of jarosite-bearing deposits through aqueous oxidation of pyrite at Meridiani Planum, Mars, *Geophys. Res. Lett.*, *32*, L21203, doi:10.1029/2005GL024253.

T. D. Glotch and H. B. Jensen, Department of Geological Sciences, State University of New York at Stony Brook, Stony Brook, NY 11794–2100, USA. (hjensen@ic.sunysb.edu; fax, (631) 632–8240)